Broadband Transmit/Receive Switch for 3T and 7T Magnetic Resonance Imaging

Ashraf Abuelhaija[1],[*] ⓘ · Gameel Saleh[2] ⓘ · Sanaa Salama[3] ⓘ · Mohammed Hamdan[1] ⓘ

Abstract

This article presents a transmit/receive switch that utilizes a broadband microstripline hybrid coupler. The proposed switch is suitable for application in both 3T and 7T magnetic resonance imaging. It operates within three frequency ranges, covering well-known X-atomic nuclei, such as ^{1}H, ^{13}C, ^{19}F, ^{23}Na, and ^{31}P, at both 3T and 7T magnetic field strengths. For the 7T application, the switch simultaneously covers the corresponding X-atomic nuclei frequencies within two bands. However, for the 3T application, tuning is required to cover the corresponding X-atomic nuclei frequencies, particularly those below 60 MHz. The microstripline trace widths of the proposed switch were designed to prevent excessive temperature increases when exposed to 1 kW power of radio frequency pulses. The characteristics of the switch were obtained using the Momentum tool—an electromagnetic simulator supported by ADS software. The proposed switch was fabricated, with its measurement verification results demonstrating favorable return loss (>10 dB), high isolation (>40 dB), and low insertion loss (<0.8 dB) at all operating frequencies.

Key Words: Broadband, Hybrid Coupler, Magnetic Resonance Imaging, Microstripline, PIN Diode.

I. INTRODUCTION

Magnetic resonance spectroscopy holds great promise in clinical neurological practice. It measures the concentrations of specific chemicals in the body to help diagnose diseases in the brain and other cancerous tissues. Cancerous tissues are often characterized by metabolic alterations. Notably, ^{13}C magnetic resonance imaging (MRI) examines variations in the metabolism of organic molecules. These changes in biochemical processes serve as a marker for the presence of certain disorders, including prostate cancer, brain tumors, diabetes, lung injury, neuroinflammation, inflammatory arthritis, cardiovascular disease, and cardiac metabolism [1]. Specifically, brain tumors are commonly detected by ^{31}P MRI scanner assessments of phosphorous composition and cellular energy [2]. Likewise, breast cancer can be diagnosed by ^{23}Na MRI, which detects changes in ion homeostasis, since the total concentration of sodium is notably higher in malignant breasts than in healthy tissues. It also allows the visualization of tissue ^{23}Na concentrations for patients with lung cancer [3]. Furthermore, ^{31}P MRI has been found to be feasible for use as a measure of tongue cancer in 7T MRI [4]. Additionally, ^{13}C MRI is suitable both for initial diagnosis and for monitoring the treatment of prostate cancer [5]. In this context, X-nuclei switches and coils enable physicians to study metabolism and measure chemical transformation, since they can help characterize the sophistication of tissues or the chemical consequences of disease progression [6, 7].

The switches used in MRI transmit radio frequency (RF) signals from an RF amplifier to the body through an RF coil, and also receive the signal from the body through the RF coil to then redirect it to the receiver circuit. Single- and multi-tuned switches are used for single- and multi-resonant coils, respectively. Notably, several methods for designing these switches have already been developed, such as trap circuits, positive-intrinsic-negative (PIN) diodes, transistors, and microelectromechanical systems (MEMS). In [8], a PIN diode-based ^{1}H transmit/receive (T/R) switch was introduced, owing to its reliability and linearity, to achieve a reduction in the switching time to 1 microsecond. In [9], a dual-tuned T/R switch capable of handling both ^{1}H and ^{31}P frequencies was engineered specifically for 3T MRI applications. This circuit, which included a linear switch for the ^{1}H coil and a quadrature switch for the ^{31}P coil, employed PIN diodes in conjunction with various other electronic components. Field effective transistor (FET)-based switches have been introduced as another topology and solution for switches in MRI [10–12]. For instance, a depletion-mode gallium nitride (GaN) switch was introduced in [11], while an enhanced-mode GaN (eGaN) FET-based switch was proposed in [12]. These switches have advantages over PIN diode switches in terms of their low DC power and reduced amount of biasing current used. However, FET switches are sensitive to RF power overstress and temperature [11], and they often suffer from lower signal-to-noise ratio (SNR) [12]. To address this, MEMS-based switches were introduced to MRI coils in [13, 14]. Notably, dual-tuned switches based on MEMS and PIN diodes, used along with a dual-tuned ^{1}H/^{19}F coil, were investigated for lung MRI applications [15]. The MEMS switch demonstrated reduced DC switching voltage compared to PIN diodes in a reverse bias state [16].

Microstripline (MSL)-based switches represent a novel switch category whose advantages over conventional couplers lie in their enhanced heat dissipation and ability to manage higher power signals [17]. A compact dual-tuned MSL-based switch designed for a dual-resonant ^{1}H/^{13}C coil was introduced for 7T MRI in [18]. This innovative design accommodated simultaneous dual-frequency signal transmission to and from a dual-resonance RF coil, eliminating the need for tuning during operation. Moreover, in [18], the size of the switch was reduced by 50% compared to the initial ^{1}H MSL-based switch in [17]. In [19], two MSL-based switches were introduced—one to interrogate different X-nuclei (^{1}H, ^{13}C, ^{19}F, ^{23}Na, and ^{31}P) one at a time by tuning, and the second to work as a dual-tuned switch for ^{1}H/^{23}Na MRI applications. Furthermore, a dual-tuned ^{1}H/^{31}P quadrature MSL-based T/R switch for 7T MRI was introduced in [20]. A single ^{1}H MSL-based switch for 7T MRI, bearing a T- and cascaded pi-shape and a realistic MSL trace width, was designed and extensively investigated to specify exact widths without in-creasing the temperature [21]. In [22, 23], two geometries of broadband MSL-based switches were introduced to simultaneously cover the X-nuclei (^{1}H, ^{13}C, ^{19}F, ^{23}Na, and ^{31}P) for 7T MRI without tuning. All of these MSL-based switches demonstrate excellent characteristics, including strong signal matching, high isolation, minimal insertion loss, effective power dissipation, and the capacity to manage high-power signals.

The novelty of this specific switch design lies in its ability to work along with RF coils to cover resonances corresponding to a wide range of X-nuclei for both 3T and 7T MRI. From an economic perspective, such a design does away with the need to use different switches with different coils since the same switch can be used for different MRI machines. This reduces both costs and complexity while also keeping sufficient space to facilitate future designs of multichannel-multi resonant coils that can be used for both 3T and 7T MRI simultaneously.

II. The Proposed Broadband T/R Switch

1. Overview of the T/R Switch

A T/R switch is considered an important device in an MRI system that utilizes T/R RF coils. In the transmission state, after generating a pulsed RF signal, an RF signal is fed into a power amplifier to amplify it to the necessary level for exciting the intended X-nuclei. Following this, the T/R switch transmits the RF signal to the RF coil. At the reception state, the RF coil delivers the detected signal from the targeted object to the T/R switch, which in turn forwards it to the low-noise amplifier, as shown in Fig. 1.

2. Broadband Hybrid Couplers

Due to growing interest in high-speed wireless communication, the demand for ultra-wideband (UWB) technology and devices has increased manifold. Notably, classical quadrature hybrid couplers demonstrate narrowband characteristics. Therefore, in recent years, several studies and investigations have been conducted on couplers to extend their bandwidths [24–28]. In [24], a two-section wideband hybrid coupler using a short-circuited parallel-coupled 3-line was presented. This coupler exhibited 55% fractional bandwidth (FBW) under specifica-
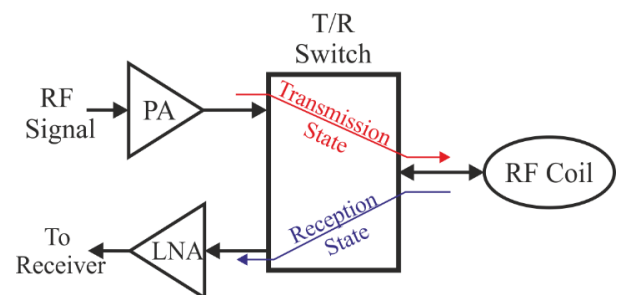

Fig. 1. Simplified diagram of an integrated T/R switch in an MRI system.

tions limited by 1 dB power imbalance, 20.1 dB return loss, 20.8 dB isolation, and 3.2° phase imbalance. In [25], a hybrid coupler using a tandem connection was presented, demonstrating 38% FBW under specifications limited by 0.6 dB power imbalance, 25 dB return loss, and 32 dB isolation. Under the same conditions as the tandem coupler, a UWB hybrid coupler was designed using the tandem connection between two 8.3 dB multi-section couplers [26] to be used in the frequency range from 1 GHz to 10 GHz. It was designed under specifications limited by ±1.5 dB amplitude unbalance, $\pm7°$ phase imbalance, and both isolation and return loss of more than 14 dB. In [27], an UWB multilayer 3 dB directional coupler was presented, whose operating frequency extended from 3.1 GHz to 10.6 GHz, with a coupling and insertion loss of 3.4 dB $\pm$ 1.1 dB. The isolation and return loss were more than 14 dB. In [28], a 3-dB UWB coupler using multilayer technology, operating between 3.1 and 10.6 GHz, was presented. It was designed under specifications limited by ±1.3 dB amplitude unbalance, 3.5° phase unbalance, 19 dB return loss, and 18 dB isolation.

The broadband 3T and 7T T/R switch proposed in this study can cover frequencies corresponding to the common X-nuclei resonant frequencies at 3T and 7T MRI, summarized in Table 1. While resonances above 61 MHz fall within the two broadbands offered by the switch without the need for tuning, the lower frequencies can be covered after applying the tuning method.

3. Methods and Materials

The 3T and 7T T/R switch presented in this study was designed based on a two-section branch-line hybrid coupler, initially introduced in [29]. Such a coupler is constructed using two sections of transmission lines, consisting of three vertical lines (*a*, *c*, *a*) and four identical horizontal lines (*b*, *b*, *b*, *b*). These lines share a common vertical line connected to an inverter, as illustrated in Fig. 2. Notably, the quarter-wavelength is the standardized length employed for all the vertical and horizontal lines. In this context, the characteristic impedance of transmission line a can be determined using the formula described in [29].

$$Z_a = (\sqrt{k} + \sqrt{k+1})Z_o. \tag{1}$$

Here, k represents the ratio of the signal power at port 2 (through) to the signal power at port 4 (coupled), and Z_o is the port impedance, which is typically 50 Ω. When k equals 1, the input signal inserted at port 1 is evenly divided between ports 2 and 4, along with a 90° phase shift, resulting in −3 dB quadrature outputs, while port 3 remains isolated. This configuration corresponds to a 90° hybrid coupler. Substituting k with 1 in Eq. (1), Z_a becomes 2.414 times Z_o. Therefore, to calculate the characteristic impedances of transmission lines *b* and *c*, the following formula, as described in [29], can be employed:

$$k = \frac{Z_o^2 Z_c^2}{Z_b^4}. \tag{2}$$

On rearranging Eq. (2), the following equation will be obtained:

$$Z_c = \frac{\sqrt{k} Z_b^2}{Z_o}. \tag{3}$$

Assuming Z_b is equal to Z_o, Z_c will also be equal to Z_o. After calculating the characteristic impedances, the following values can be achieved: Z_a = 120.7 Ω and $Z_b = Z_c$ = 50 Ω. The simulated S-parameters of the proposed coupler are depicted in Fig. 3(a). The operational bandwidth, considering a 1 dB magnitude imbalance and a 5° phase imbalance, is determined from Fig. 3(a) and 3(b) as approximately 48.2%. Notably, for practical applications, the hybrid coupler was designed using a Rogers RO4003C substrate with a permittivity of 3.38 and a thickness of 1.52 mm. Fig. 4 depicts the layout of the hybrid coupler in a Momentum electromagnetic simulation, which is supported by ADS software.

The dimensions for each transmission line in Fig. 2 are summarized in Table 2. The operating frequency of the coupler was chosen to be 95 MHz. To reduce the overall area of the coupler, the microstrip lines were designed in a multi-bended manner. Ultimately, the dimensions of the final design were established
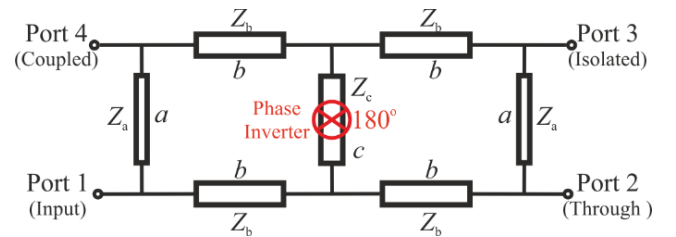

Fig. 2. Schematic diagram of the two-section branch-line hybrid coupler. Adapted from Abuelhaija and Saleh [22].

Table 1. Gyromagnetic ratio and resonant frequency at 3T and 7T for common nuclei

Nucleus	[1]H	[19]F	[31]P	[23]Na	[13]C
Gyromagnetic ratio ($\gamma/2\pi$) in MHz/Tesla	42.58	40.08	17.25	11.27	10.71
Frequency @ 3T in MHz	127.74	120.24	51.75	33.81	32.13
Frequency @ 7T in MHz	298.06	280.56	120.75	78.89	74.97
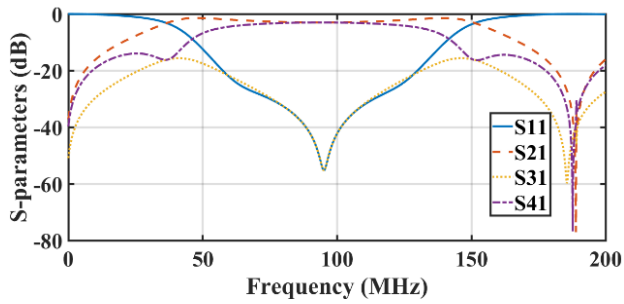
(a)
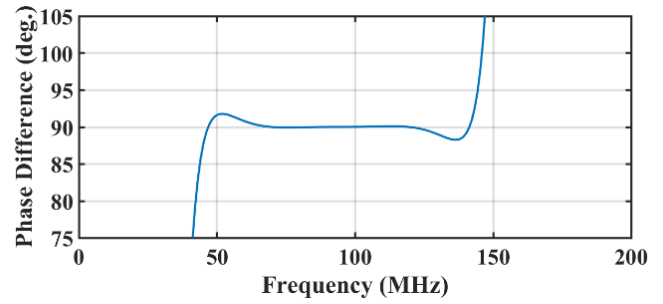
(b)

Fig. 3. (a) Simulated *S*-parameters of the two-section branch-line hybrid coupler with *k* = 1 and (b) phase difference between the through and coupled ports.

Fig. 4. Layout of the two-section branch-line hybrid coupler.

Table 2. Dimensions of the hybrid coupler microstriplines designed at 95 MHz
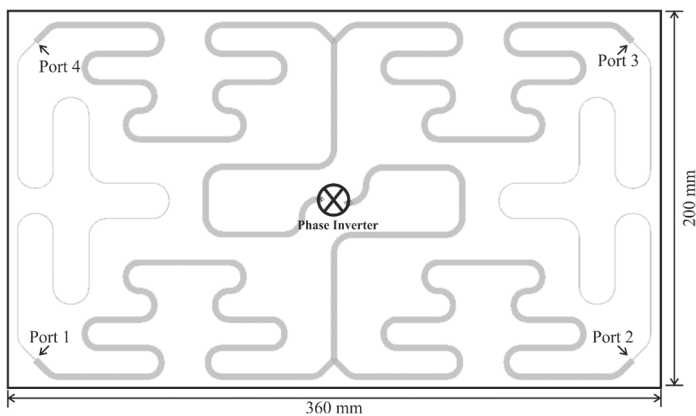
	Transmission line					
	a		*b*		*c*	
	l_a	W_a	l_b	W_b	l_c	W_c
Dimension (mm)	509	0.53	482.5	3.51	482.5	3.51

as 360 mm × 200 mm, which reduced the size of the coupler by 62.7% in comparison to the coupler without bending.

The hybrid coupler assumed a pivotal role in the design of the broadband 3T and 7T T/R switch. As depicted in Fig. 5, the proposed T/R switch comprises two hybrid couplers—while the left coupler is dedicated to the transmission state, both are simultaneously engaged in the reception state. In the transmission state, a pulsed RF signal is fed into port 1 and subsequently forwarded to the RF coil at port 2 after applying forward bias to the PIN diodes. During reception, both PIN diodes are reverse-biased, facilitating the routing of the detected signal from the RF coil to the receiver at port 4. To minimize the overall footprint of the T/R switch, both couplers were positioned in a back-to-back configuration, ensuring a common ground connection. The coupled and through ports of the first coupler were
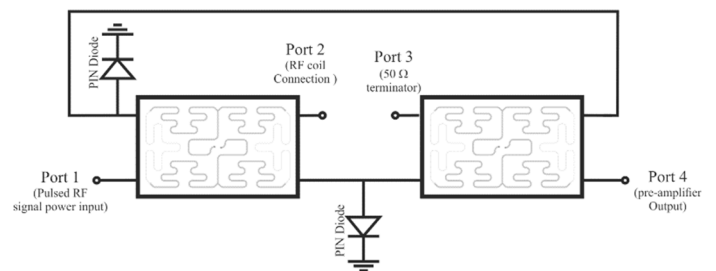

Fig. 5. Two-section branch-line hybrid coupler based broadband T/R switch.

internally connected to the corresponding ports in the second coupler using small connectors. A phase inverter (180° phase shifter) was inserted in the middle of each coupler using a coaxial cable on a crossover configuration.

To cover the frequencies of 7T MRI and the most common X-nuclei resonant frequencies at 3T MRI without the need for tuning, the operating frequency of the couplers was chosen to be 95 MHz. At this frequency, the T/R switch would be able to cover frequencies of X-nuclei that are more than 61 MHz within its two broadbands. The resonance frequencies corresponding to the remaining X-nuclei (such as ^{31}P, [23]Na, and ^{13}C at 3T) for 3T MRI can also be covered by adding a tuning capacitor $C_t =$ 62 pF at the terminals of each MSL, as shown in Fig. 6. For the middle MSL *c*, the quarter-wavelength MSL was split into two-eighth of an MSL, with a phase inverter in between. Each eighth MSL was connected to one tuning capacitor with a value of $2 \times C_t$ from one terminal.

III. SIMULATION RESULTS AND MEASUREMENT VERIFICATION

1. Simulation Results

The *S*-parameters obtained by conducting EM simulations using the designed hybrid coupler (see Fig. 4) are shown in Fig. 7. The coupler was characterized by two broadbands—the first extended around the fundamental frequency (95 MHz), whereas the second extended around the third odd harmonics (285
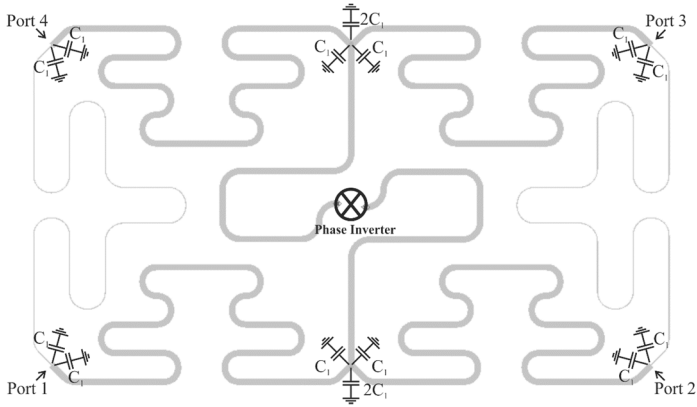
Fig. 6. Layout of the two-section branch-line hybrid coupler with tuning capacitors.

MHz). The bandwidths of the first and second broadbands fell within the 70–120 MHz and 260–308 MHz ranges, respectively, as calculated based on the following specifications: less than 1 dB magnitude imbalance and less than 5 phase imbalance. Notably, the proposed hybrid coupler demonstrated low return loss ($S_{11} < -25$ dB) and high isolation ($S_{31} < -25$ dB).

The evaluation of the T/R switch equipped with a two-section hybrid coupler was conducted by analyzing the S-parameters acquired from the electromagnetic simulations. As depicted in Fig. 8 and Tables 3 and 4, in the transmission state, the T/R switch exhibits commendable performance, characterized by strong matching ($S_{11} < -10$ dB) and minimal insertion loss ($S_{21} > -0.56$ dB) across all X-nuclei frequencies. Further-
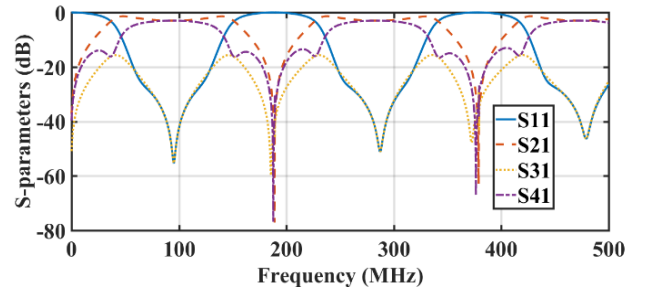

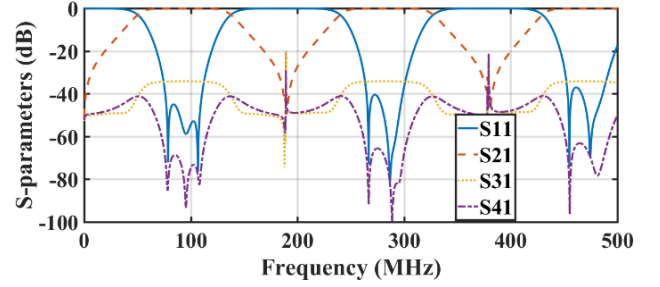Fig. 7. S-parameters for the two-section branch-line hybrid couplers.

Fig. 8. S-parameters of the broadband T/R switch in the transmission state.

more, substantial isolation ($S_{41} < -44$ dB) between port 1 (the signal generator) and port 4 (the receiver) was achieved. Furthermore, as illustrated in Fig. 9 and Tables 3 and 4, the T/R switch maintains favorable matching ($S_{22} < -23.9$ dB) and low insertion loss ($S_{42} < -0.32$ dB) at all X-nuclei frequencies in the reception state.

Table 3. Simulated S-parameters of the broadband T/R switch in the transmission state and reception state at 3T

Atomic nuclei	Frequency (MHz)	Transmission state (dB)			Reception state (dB)		
		S_{11}	S_{21}	S_{41}	S_{22}	S_{12}	S_{42}
^{1}H	127.74	−10.60	−0.56	−44.70	−25.45	−22.36	−0.32
^{19}F	120.24	−20 .17	−0.21	−52.30	−26.87	−23.57	−0.12
^{31}P	51.75	–	–	–	–	–	–
^{23}Na	33.81	–	–	–	–	–	–
^{13}C	32.13	–	–	–	–	–	–

Table 4. Simulated S-parameters of the broadband T/R switch in the transmission state and reception state at 7T

Atomic nuclei	Frequency (MHz)	Transmission state (dB)			Reception state (dB)		
		S_{11}	S_{21}	S_{41}	S_{22}	S_{12}	S_{42}
^{1}H	298.06	−43.12	−0.17	−75.50	−28.52	−30.41	−0.02
^{19}F	280.56	−48.00	−0.17	−67.80	−41.25	−33.06	−0.01
^{31}P	120.75	−19.25	−0.21	−51.50	−27.50	−23.48	−0.13
^{23}Na	78.89	−55.40	−0.17	−85.00	−25.32	−25.97	−0.04
^{13}C	74.97	−33.34	−0.17	−63.75	−23.90	−24.35	−0.07

Fig. 8 depicts the two broadbands of the T/R switch in the transmission state. The first band extends from 61.1 MHz to 128.3 MHz, while the second band extends from 250.3 MHz to 317.5 MHz. They were calculated based on specifications of less than 1 dB insertion loss and less than 10 dB return loss. Furthermore, Fig. 9 presents the two broadbands of the T/R switch at the reception state. It is observed that the insertion loss for both bands is less than 0.36 dB, while the return loss is less than 23.5 dB.

To address the remaining X-nuclei frequencies, the hybrid couplers in the T/R switch were tuned using capacitor C_t. During transmission, the T/R switch achieved excellent matching ($S_{11} < -21$ dB) and low insertion loss ($S_{21} > -0.35$ dB) at the remaining X-nuclei frequencies, as seen in Fig. 10 and Table 5. Furthermore, high isolation ($S_{41} < -35.9$ dB) between port 1 (signal generator) and port 4 (receiver) was achieved. In the reception state, the T/R switch maintained strong matching (S_{22}

< -11.1 dB) and low insertion loss ($S_{42} < -0.6$ dB) at these frequencies, as shown in Fig. 11 and Table 5.

2. Measurement Verification

A prototype of the two-section branch-line hybrid coupler was fabricated on a 360 mm × 200 mm Rogers RO4003C substrate with a permittivity of 3.38 and thickness of 1.52 mm, as shown in Fig. 12. The subminiature version A (SMA) connectors for each port were soldered to the bottom of the substrate. The phase inverter (180° phase shifter) in the middle of the coupler was implemented using a very short 50 Ω coaxial cable on a crossover configuration. Notably, while it is possible to add a coaxial cable of any electrical length, even 0°, in simulations, such is not the case in reality—adding a coaxial cable with 0° electrical length is not possible. As a result, in this study, differ-
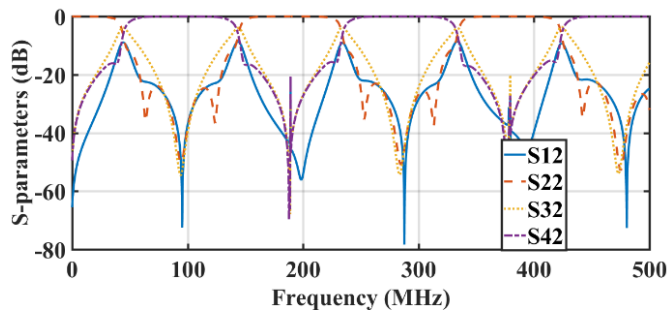

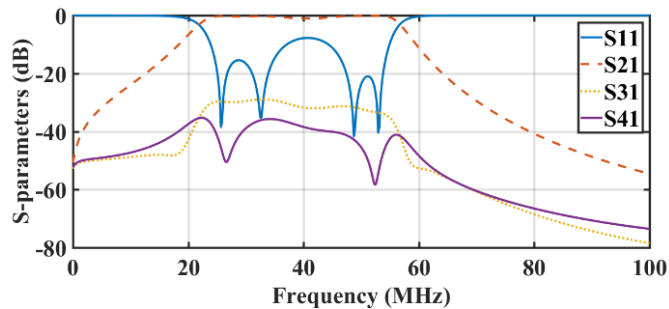Fig. 9. *S*-parameters of the broadband T/R switch in the reception state.
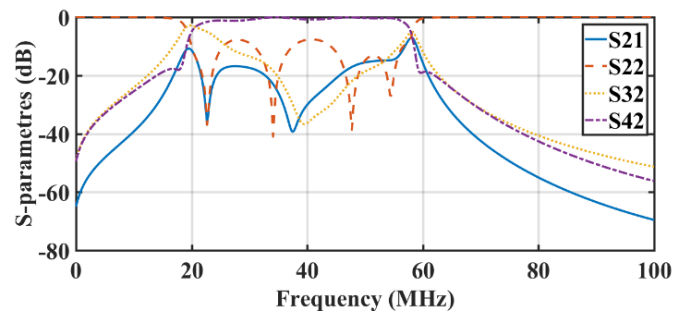
Fig. 11. *S*-parameters of the broadband T/R switch in the reception state after tuning.

Fig. 10. *S*-parameters of the broadband T/R switch in the transmission state after tuning.
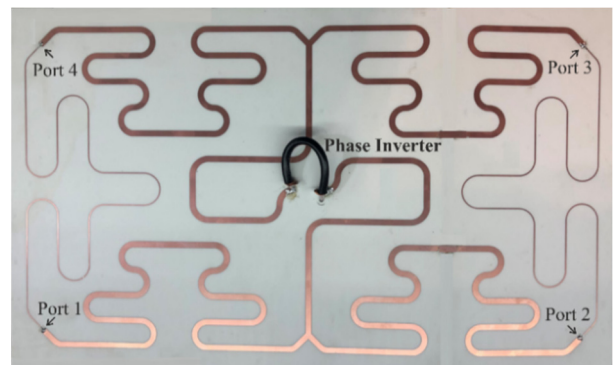
Fig. 12 Prototype of the two-section branch-line hybrid coupler.

Table 5. Simulated *S*-parameters of the broadband T/R switch in the transmission state and reception state at 3T after tuning

Atomic nuclei	Frequency (MHz)	Transmission state (dB)			Reception state (dB)		
		S_{11}	S_{21}	S_{41}	S_{22}	S_{12}	S_{42}
[1]H	127.74	–	–	–	–	–	–
[19]F	120.24	–	–	–	–	–	–
[31]P	51.75	−21.10	−0.24	−48.78	−13.40	−15.25	−0.42
[23]Na	33.81	−31.36	−0.32	−35.90	−17.55	−20.30	−0.23
[13]C	32.13	−21.06	−0.35	−37.14	−11.10	−18.25	−0.60

ent coaxial cable lengths were tested to observe their effects. The effect of the electrical length of a coaxial cable (phase inverter) on coupler characteristics is shown in Fig. 13, where it is observed that the higher the electrical length, the lower the phase shift (less than 180°). Notably, this deviation from the 180° phase shift led to increased return loss and reduced bandwidth at the third odd harmonics. Fig. 13 clearly shows that at the acceptable deviation of 10° (θ = 10°), a return loss of less than 10 dB and a bandwidth of at least 90% can be maintained, coinciding with results of the electrical length without a deviation at 180° (θ = 0°). In practice, the physical length of the connected coaxial cable corresponded to a 5° electrical length. Notably, the electrical length was calculated based on the 95 MHz fundamental frequency of the coupler.

The T/R switch was easily fabricated using two hybrid couplers, as shown in Fig. 12. They were connected back to back, so that the ground planes of the two substrates were joined. To examine the internal connections between the couplers corresponding to the connections shown in Fig. 5, two thin wires were inserted through the ground planes. Two PIN diodes were placed on the first coupler at ports 2 and 4 in the same position as the two thin wires.

Fig. 14(a) and 14(b) present the measured and simulated S-parameters of the T/R switch during transmission and reception. In the transmission state, the T/R switch shows excellent matching (S_{11} < −10 dB), low insertion loss (S_{21} > −0.8 dB), and high

isolation (S_{41} < −44 dB) between the signal generator (port 1) and the receiver (port 4) across all X-nuclei frequencies. During reception, the T/R switch maintains good matching (S_{22} < −17 dB) and low insertion loss (S_{42} > −0.4 dB) at all X-nuclei frequencies.

Fig. 15(a) and 15(b) present the measured and simulated S-parameters of the T/R switch in the transmission and reception states after using tuning capacitors. They cover the first frequency band required to cover the corresponding X-atomic nuclei frequencies, especially those below 60 MHz. Notably, a good match between the simulation and measurement results is observed.

However, the PIN diodes, lumped elements, transmission lines, biasing network, and Roger's substrate play crucial roles in contributing to the discrepancies between the measurements and simulations observed in Figs. 14 and 15.

IV. DISCUSSION

A comparison of the performance of the proposed 3T–7T T/R switch with that of state-of-the-art switches is reported in Table 6, clearly demonstrating that the proposed T/R switch shows promising performance relative to the other designs. The proposed switch can operate at three wide frequency bands: 25–55 MHz, 61.1–128.3 MHz, and 250.3–317.5 MHz. Comparatively, in [30, 31], the highest operating frequency was limited to 200 MHz. Furthermore, in [17, 32–34], the lowest operating frequencies were above 250 MHz. Therefore, all state-of-the-art
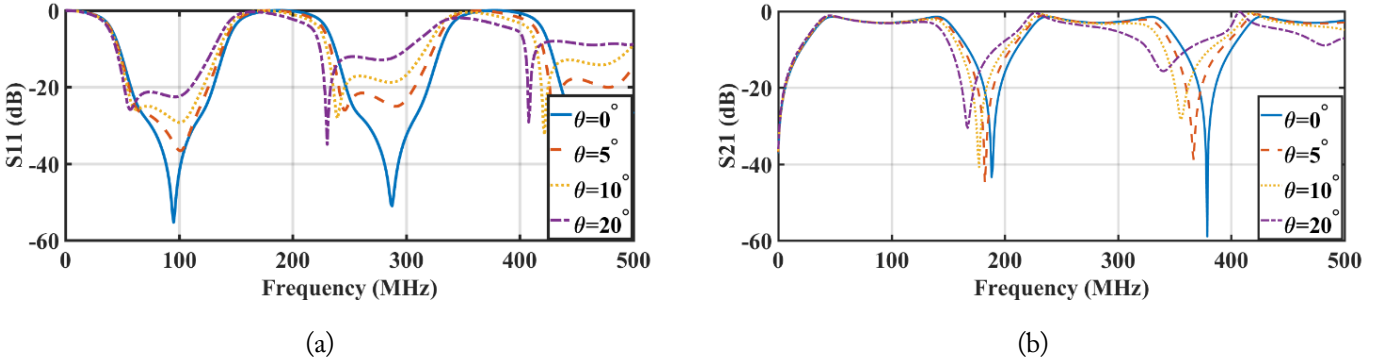
Fig. 13. Simulated (θ = 0°) and measured (θ = 5°, 10°, and 20°): (a) S_{11} and (b) S_{21} parameters for different coaxial cables.
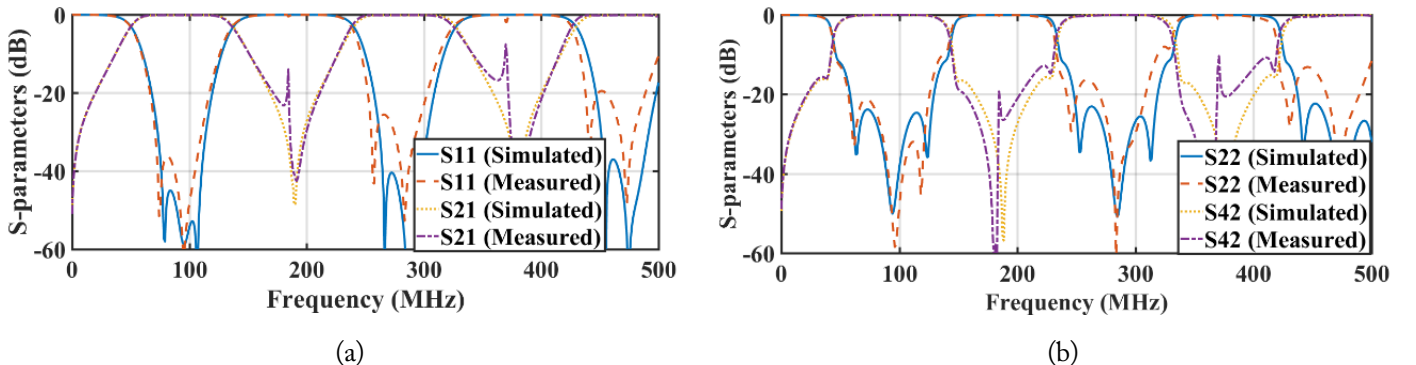

Fig.14. Measured and simulated S-parameters for two-section hybrid couplers-based T/R switch in (a) transmission state and (b) reception state.
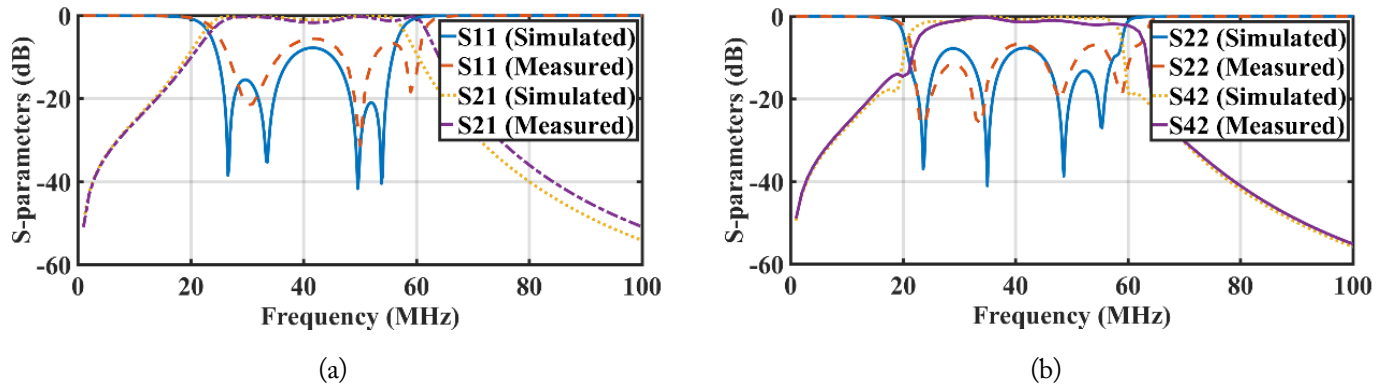
Fig. 15. Measured and simulated *S*-parameters for two-section hybrid couplers-based T/R switch in (a) transmission state after tuning and (b) reception state after tuning.

reported switches failed to cover many of the atomic X-nuclei frequencies for 3T and 7T magnetic field strengths. In addition, as shown in Table 6, the proposed switch demonstrates low insertion loss in both the transmission and reception states as compared to the designs reported in [30, 33, 34]. Regarding isolation performance, the designed switch demonstrates high isolation compared to its counterparts reported in [32–34]. Moreover, based on the performance of the proposed switch, it can be used along with both single- and multi-tuned RF coils that resonate within the three broadbands of its operating frequencies. As a result, the scanning process can be conducted without changing the type of RF coil or asking the patient to move. This will not only minimize the number of artifacts used but also reduce the amount of time spent in the scanning process.

V. Conclusion

This work involved designing, simulating, and fabricating a broadband transmit/receive switch for 3T and 7T MRI. ADS software was employed to design the switch, incorporating two hybrid couplers based on the two-section branch-line method, each with specified performance criteria (1 dB magnitude imbalance and 5° phase imbalance). The switch successfully covered various atomic X-nuclei frequencies within its three primary frequency bands (25–55 MHz, 61.1–128.3 MHz, and 250.3–317.5 MHz) at 3T and 7T magnetic field strengths, maintaining excellent return loss (>10 dB) and isolation (>40 dB), as well as low insertion loss (<0.8 dB), at all operating frequencies.

References

[1] Z. J. Wang, M. A. Ohliger, P. E. Larson, J. W. Gordon, R. A.

Table 6. Comparison between this work and the state-of-the-art T/R switches

Study	Frequency range (MHz)	Insertion loss (dB)		Tx-Rx isolation (dB)	Coil port return loss (dB)
		Transmission state	Reception state		
Yuan et al. [32]	250–1,000	0.2–0.56	0.2–0.56	>35	>13
Xiao et al. [30]	0.3–200	0.4–6	0.14–5	62–90	>22.6
Abuelhaija et al. [17]	280–340	<0.3	<0.45	>40	>20.0
Caverly [33]	290–310	1–2	–	12–28	–
Ji et al. [34]	250–350	0.2–2	0.27–2	16–35.7	–
Abou-Khousa and Mustapha [31]	30–200	0.09–0.2	0.11–0.37	63–80	>18
	(3 bands) 25–55	0.2–0.8	0.2–0.4	>40	>10
This work	61.1–128.3				
	250.3–317.5				

"-" indicates that the corresponding result has not been evaluated.

Bok, et al., "Hyperpolarized ^{13}C MRI: state of the art and future directions," *Radiology*, vol. 291, no. 2, pp. 273-284, 2019. https://doi.org/10.1148/radiol.2019182391

[2] S. B. Peter and V. R. Nandhan, "31-Phosphorus magnetic resonance spectroscopy in evaluation of glioma and metastases in 3T MRI," *Indian Journal of Radiology and Imaging*, vol. 31, no. 4, pp. 873-881, 2021. https://doi.org/10.1055/s-0041-1741090

[3] T. Henzler, S. Konstandin, G. Schmid-Bindert, P. Apfaltrer, S. Haneder, F. Wenz, et al., "Imaging of tumor viability in lung cancer: initial results using ^{23}Na-MRI," *RöFo*, vol. 184, no. 4, pp. 340-344, 2012. https://doi.org/10.1055/s-0031-1299277

[4] R. Forner, K. Nam, K. J. de Koning, T. van der Velden, W. van der Kemp, A. Raaijmakers, and D. W. Klomp, "RF coil setup for ^{31}P MRSI in tongue cancer in vivo at 7 T, " *Frontiers in Neurology*, vol. 12, article no. 695202, 2021. https://doi.org/10.3389/fneur.2021.695202

[5] UCH Clinical Trials, "Hyperpolarized Pyruvate (^{13}C) MR imaging in monitoring patients with prostate cancer on active surveillance," 2024 [Online]. Available: https://clinicaltrials.ucbraid.org/trial/NCT03933670.

[6] J. Dai, M. Gosselink, T. A. van der Velden, E. F. Meliado, A. J. E. Raaijmakers, and D. W. J. Klomp, "An RF coil design to enable quintuple nuclear whole-brain MRI," *Magnetic Resonance in Medicine*, vol. 89, no. 5, pp. 2131-2141, 2023. https://doi.org/10.1002/mrm.29577

[7] C. Ianniello, G. Madelin, L. Moy, and R. Brown, "A dual-tuned multichannel bilateral RF coil for ^{1}H/^{23}Na breast MRI at 7 T," *Magnetic Resonance in Medicine*, vol. 82, no. 4, pp. 1566-1575, 2019. https://doi.org/10.1002/mrm.27829

[8] D. O. Brunner, L. Furrer, M. Weiger, W. Baumberger, T. Schmid, J. Reber, et al., "Symmetrically biased T/R switches for NMR and MRI with microsecond dead time," *Journal of Magnetic Resonance*, vol. 263, pp. 147-155, 2016. https://doi.org/10.1016/j.jmr.2015.12.016

[9] B. Thapa, J. Kaggie, N. Sapkota, D. Frank, and E. K. Jeong, "Design and development of a general-purpose transmit/receive (T/R) switch for 3T MRI, compatible for a linear, quadrature and double-tuned RF coil," *Concepts in Magnetic Resonance Part B: Magnetic Resonance Engineering*, vol. 46, no. 2, pp. 56-65, 2016. https://doi.org/10.1002/cmr.b.21321

[10] P. K. Grannell, M. J. Orchard, P. Mansfield, A. N. Garroway, and D. C. Stalker, "A FET analogue switch for pulsed NMR receivers," *Journal of Physics E: Scientific Instruments*, vol. 6, no. 12, article no. 1202, 1973. https://doi.org/10.1088/0022-3735/6/12/020

[11] J. Y. Lu, T. Grafendorfer, T. Zhang, S. Vasanawala, F. Robb, J. M. Pauly, and G. C. Scott, "Depletion-mode GaN HEMT Q-spoil switches for MRI coils," *IEEE Transactions on Medical Imaging*, vol. 35, no. 12, pp. 2558-2567, 2016. https://doi.org/10.1109/TMI.2016.2586053

[12] M. Twieg, M. D. Rooij, and M. A. Griswold, "Enhancement mode GaN on silicon (eGaN FETs) for coil detuning," in *Proceedings of the Joint Annual Meeting ISMRM–ESMRMB*, Milan, Italy, 2014.

[13] M. Fuentes, E. Weber, S. Wilson, B. Li, and S. Crozier, "Micro-electromechanical systems (MEMS) based RF-switches in MRI: a performance study," in *Proceedings of the 18th Annual Meeting of ISMRM*, Stockholm, Sweden, 2010.

[14] S. B. Bulumulla, K. J. Park, E. Fiveland, J. Iannotti, and F. Robb, "MEMS switch integrated radio frequency coils and arrays for magnetic resonance imaging," *Review of Scientific Instruments*, vol. 88, no. 2, article no. 025003, 2017. https://doi.org/10.1063/1.4975181

[15] A. Maunder, M. Rao, F. Robb, and J. Wild, "RF coil design for multinuclear lung MRI of 19F fluorinated gases and 1H using MEMS," in *Proceedings of the 24th Annual Meeting of ISMRM,* Singapore, 2016.

[16] A. Maunder, M. Rao, F. Robb, and J. M. Wild, "Comparison of MEMS switches and PIN diodes for switched dual tuned RF coils," *Magnetic Resonance in Medicine*, vol. 80, no. 4, pp. 1746-1753, 2018. https://doi.org/10.1002/mrm.27156

[17] A. Abuelhaija, G. Saleh, T. Baldawi, and S. Salama, "Symmetrical and asymmetrical microstripline-based transmit/receive switches for 7-Tesla magnetic resonance imaging," *International Journal of Circuit Theory and Applications*, vol. 49, no. 7, pp. 2082-2093, 2021. https://doi.org/10.1002/cta.3013

[18] G. Saleh and A. Abuelhaija, "Dual tuned switch for dual resonance 1H/13C MRI coil," in *Proceedings of 2021 IEEE International IOT, Electronics and Mechatronics Conference (IEMTRONICS)*, Toronto, Canada, 2021, pp. 1-7. https://doi.org/10.1109/IEMTRONICS52119.2021.9422627

[19] A. Abuelhaija, G. Saleh, O. Nashwan, S. Issa, and S. Salama, "Multi-and dual-tuned microstripline-based transmit/receive switch for 7-Tesla magnetic resonance imaging" *International Journal of Imaging Systems and Technology*, vol. 32, no. 2, pp. 590-599, 2022. https://doi.org/10.1002/ima.22634

[20] A. Abuelhaija and G. Saleh, "Dual tuned 1H/31P quadrature microstripline-based transmit/receive switch for 7 Tesla magnetic resonance imaging," *International Journal of Electrical & Computer Engineering*, vol. 12, no. 3, pp. 2177-2183, 2022. https://doi.org/10.11591/ijece.v12i3.pp2177-2183

[21] A. Abuelhaija and G. Saleh, "A pi-shaped compact dual tuned H/23 Na microstripline-based switch for 7-Tesla MRI," *International Journal on Communications Antenna and Propagation*, vol. 11, no. 1, pp. 57-64, 2021. https://doi.org/10.15866/irecap.v11i1.20302

[22] A. Abuelhaija and G. Saleh, "Two-section branch-line hybrid couplers based broadband transmit/receive switch," *International Journal of Electrical and Computer Engineering (IJECE)*, vol. 13, no. 3, pp. 2600-2607, 2023. https://

doi.org/10.11591/ijece.v13i3.pp2600-2607

[23] A. Abuelhaija and G. Saleh, "Broadbands four-branch hybrid coupler-based T/R switch for 7-Tesla magnetic resonance imaging," *International Journal on Communications Antenna and Propagation*, vol. 12, no. 5, pp. 380-384, 2022. https://doi.org/10.15866/irecap.v12i5.22449

[24] H. J. Yoon and B. W. Min, "Two section wideband 90° hybrid coupler using parallel-coupled three-line," *IEEE Microwave and Wireless Components Letters*, vol. 27, no. 6, pp. 548-550, 2017. https://doi.org/10.1109/LMWC.2017.2701304

[25] A. Jain, R. P. Yadav, and S. V. Kulkarni, "Design and development of 2 kW, 3 dB hybrid coupler for the prototype ion cyclotron resonance frequency (ICRF) system," *International Journal of Microwave and Wireless Technologies*, vol. 11, no. 1, pp. 1-6, 2019. https://doi.org/10.1017/S175907871800137X

[26] S. M. H. Javadzadeh, S. M. S. Majedi, and F. Farzaneh, "Broadside coupler channels 1 to 10 GHz," *Microwaves and RF*, vol. 51, no. 1, pp. 68-77, 2012.

[27] M. Leib, D. Mack, F. Thurow, and W. Menzel, "Design of a multilayer ultra-wideband directional coupler," in *Proceedings of the German Microwave Conference*, Hamburg, Germany, 2018, pp. 1-4.

[28] D. N. A. Zaidel, S. K. A. Rahim, N. Seman, C. L. Chew, and N. H. Khamis, "A design of octagon-shaped 3-dB ultra wideband coupler using multilayer technology," *Microwave and Optical Technology Letters*, vol. 55, no. 1, pp. 127-130, 2013. https://doi.org/10.1002/mop.27259

[29] L. Chiu and Q. Xue, "Wideband parallel-strip 90 hybrid coupler with swap," *Electronics Letters*, vol. 44, no. 11, pp. 687-688, 2018. https://doi.org/10.1049/el:20080975

[30] Y. Xiao, Z. Zhao, Z. Qian, and H. Zhou, "A high isolation switching unit for MRI system," *Procedia Engineering*, vol. 7, pp. 265-269, 2010. https://doi.org/10.1016/j.proeng.2010.11.042

[31] M. A. Abou-Khousa and A. A. Mustapha, "Wideband RF transmit-receive switch for multi-nuclei NMR spectrometers," *IEEE Transactions on Circuits and Systems II: Express Briefs*, vol. 69, no. 3, pp. 904-908, 2022. https://doi.org/10.1109/TCSII.2021.3121210

[32] L. Yuan, Z. Wang, W. Wei, and X. Han, "High-frequency broadband RF transmit-receive switch for pulsed magnetic field NMR," *IEEE Transactions on Instrumentation and Measurement*, vol. 72, article no. 6004109, 2023. https://doi.org/10.1109/TIM.2023.3267530

[33] R. H. Caverly, "PIN diode-based transmit-receive switch for 7 T MRI," in *Proceedings of 2016 IEEE Topical Conference on Biomedical Wireless Technologies, Networks, and Sensing Systems (BioWireleSS)*, Austin, TX, USA, 2016, pp. 100-102. https://doi.org/10.1109/BIOWIRELESS.2016.7445574

[34] Y. Ji, W. Hoffmann, M. Pham, A. E. Dunn, H. Han, C. Ozerdem, et al., "High peak and high average radiofrequency power transmit/receive switch for thermal magnetic resonance," *Magnetic Resonance in Medicine*, vol. 80, no. 5, pp. 2246-2255, 2018. https://doi.org/10.1002/mrm.27194

Ashraf Abuelhaija
https://orcid.org/0000-0002-6645-3833

is an associate professor in the Department of Electrical Engineering at Applied Science Private University, Amman, Jordan, from where he received his B.Sc. degree in communications and electronics engineering in 2007. He received his master's degree and Ph.D. in electrical engineering from DuisburgEssen University in 2010 and 2016, respectively. His research interests pertain to the area of antennas and RF technology. From 2012 to 2014, he worked as a research assistant at Erwin L. Hahn Institute for Magnetic Resonance Imaging, Essen. From 2014 to 2016, he was a research assistant at the Department of Microwave and RF Technology at Duisburg-Essen University.

Gameel Saleh
https://orcid.org/0000-0003-1502-3582
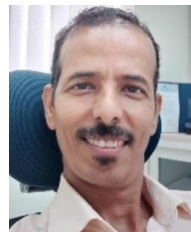
was born in Aden, Yemen. He received his B.Sc. degree in electrical engineering from Aden University, Aden, Yemen, in 2001, and his M.S. degree in electrical engineering from Jordan University of Science and Technology, Irbid, Jordan, in 2008. In 2013, he was awarded a Dr.-Ing (Ph.D.) degree in electrical engineering by Duisburg–Essen University, Duisburg, Germany. From 2014 to 2015, Dr. Saleh worked in the Communication Engineering Department of Aden University. Since 2015, he has been working as an associate professor in the Department of Biomedical Engineering at Imam Abdulrahman Bin Faisal University, Dammam, Saudi Arabia. His current research interests include RF circuits, metamaterials, wearable antennas, and biosensors. Dr. Saleh was a recipient of the German Academic Exchange Service Fellowships in 2006 and 2009.

Sanaa Salama

https://orcid.org/0000-0001-9480-6985

received her B.Sc. degree in Telecommunication Technology from the Arab American University (AAUP), Palestine, in 2006 (excellent evaluation, GPA 3.96/4), and her M.Sc. degree in electrical engineering from the University of Jordan, Jordan, in 2009 (excellent evaluation, GPA 3.83/4). In 2015, she received her Ph.D. degree in electrical engineering from Duisburg-Essen University in Germany. Her research interests include characteristic chassis wave modes, MIMO antenna design, beam-forming antenna array design, reconfigurable antennas, coupling element-based antenna structures, mutual coupling, chassis wave-mode coupling, and port and pattern isolation. Her recent field of research is the design of RF coils for 7 T MRI systems, design of decoupling and matching networks, and the design of implantable antennas for MICS and ISM bands. Since 2015, she has been an assistant professor in the Department of Telecommunication Engineering at AAUP. She has also authored a number of conference and journal papers.

Mohammed Hamdan

https://orcid.org/0000-0001-5320-2931

received his Ph.D. degree in electrical engineering from the University of Southampton, Southampton, UK, in 2019. He received his M.Sc. degree in Energy and Sustainability with Electric Power Engineering from the University of Southampton, UK, in 2014. He received his B.Sc. degree in electrical engineering from Jordan University of Science and Technology, Irbid, Jordan, in 2010. Currently, he is an assistant professor at Applied Science Private University, Jordan. His current research focuses on the impact of renewable technologies on the distribution grid, numerical simulation (FEA), and theoretical analytics (thermal, electrical, and mechanical) of high voltage AC and DC power cables.